Tuning THz emission properties of $Bi_2Sr_2CaCu_2O_{8+}$ intrinsic Josephson junction stacks by charge carrier injection

2017 Supercond. Sci. Technol. 30 034006

(http://iopscience.iop.org/0953-2048/30/3/034006)

IOP Publishing Superconductor Science and Technology
Supercond. Sci. Technol. **30** (2017) 034006 (7pp) https://doi.org/10.1088/1361-6668/aa55ae

Tuning THz emission properties of $Bi_2Sr_2CaCu_2O_{8+\delta}$ intrinsic Josephson junction stacks by charge carrier injection

O Kizilaslan[1,2], F Rudau[1], R Wieland[1], J S Hampp[1], X J Zhou[3,4], M Ji[3,4], O Kiselev[5], N Kinev[5], Y Huang[3,4], L Y Hao[4], A Ishii[3], M A Aksan[6], T Hatano[3], V P Koshelets[5], P H Wu[4], H B Wang[3,4], D Koelle[1] and R Kleiner[1]

[1] Physikalisches Institut and Center for Quantum Science (CQ) in LISA$^+$, Universität Tübingen, D-72076 Tübingen, Germany
[2] Inonu University, Department of Biomedical Engineering, Faculty of Engineering 44280, Malatya, Turkey
[3] National Institute for Materials Science, Tsukuba 3050047, Japan
[4] Research Institute of Superconductor Electronics, Nanjing University, Nanjing 210093, People's Republic of China
[5] Kotel'nikov Institute of Radio Engineering and Electronics, Russia
[6] Inonu University, Faculty of Arts and Sciences, Department of Physics, 44280 Malatya, Turkey

E-mail: olcay.kizilaslan@inonu.edu.tr

Received 9 November 2016, revised 14 December 2016
Accepted for publication 23 December 2016
Published 1 February 2017

Abstract

We report on doping and undoping experiments of terahertz (THz) emitting intrinsic Josephson junction stacks, where the change in charge carrier concentration is achieved by heavy current injection. The experiments were performed on stand-alone structures fabricated from a $Bi_2Sr_2CaCu_2O_{8+\delta}$ single crystal near optimal doping. The stacks contained about 930 intrinsic Josephson junctions. On purpose, the doping and undoping experiments were performed over only a modest range of charge carrier concentrations, changing the critical temperature of the stack by less than 1 K. We show that both undoping and doping is feasible also for the large intrinsic Josephson junction stacks used for THz generation. Even moderate changes in doping introduce large changes in the THz emission properties of the stacks. The highest emission power was achieved after *doping* a pristine sample.

Keywords: charge carrier injection, superconductors, Josephson junctions, THz emission

(Some figures may appear in colour only in the online journal)

1. Introduction

In the high-temperature superconductor $Bi_2Sr_2CaCu_2O_{8+\delta}$ (BSCCO) superconductivity is restricted to the 0.3 nm thick CuO_2 sheets which are separated by SrO and BiO barrier layers to intrinsically form a 1.5 nm thick Josephson junction [1]. Thus, a single crystal of 1 μm thickness forms a stack of ~670 intrinsic Josephson junctions (IJJs). Suitably patterned stacks emit coherent radiation at terahertz (THz) frequencies [2–4]. The emitted frequency f_e follows the Josephson relation $f_e = V_J/\Phi_0$, where Φ_0 is the flux quantum and $\Phi_0^{-1} \approx 483.6\ \mathrm{GHz\ mV^{-1}}$. V_J is the voltage across a single junction. THz radiation from IJJ stacks became a hot topic in recent years both in terms of experiment [5–36] and theory [37–61]; for recent reviews, see [3, 4]. IJJ stacks used for THz emission are often rectangular in shape, with lateral dimensions around $300 \times 50\ \mu\mathrm{m}^2$, and contain typically 500–2000 junctions. The stacks have been patterned as mesas on top of BSCCO base crystals and also as bare IJJ stacks contacted by Au layers (GBG structures) [16, 17, 20, 22] and as all-superconducting *Z*-shaped structures [11]. Emission frequencies range from 0.4–2.4 THz [30]. For the best stacks, an

emission power P_e in the range of tens of μW has been achieved [17, 19, 20, 30], and arrays of mesas showed emission with P_e up to 0.61 mW [19].

The IJJ stacks are affected by Joule heating [2, 5–8, 13, 18, 21, 24, 28, 49, 52–54, 59]. For sufficiently low bias currents, the temperature rises only slightly to values above the bath temperature T_b and the voltage V across the stack increases with increasing bias current I. With increasing I and input power the current–voltage characteristics (IVCs) start to back-bend and, at some bias current in the back-bending region, a hot spot forms in the stack [5, 6, 8, 13, 18, 21, 23, 24, 32], creating a region which is heated to temperatures above the critical temperature T_c. In the IJJ stacks one can thus distinguish a low-bias regime where the temperature in the stack varies only weakly and a high-bias regime where the hot spot has formed. THz emission can be observed in both regimes.

Almost all THz emitting IJJ stacks were based on slightly underdoped BSCCO, with the exception of [33], where Bi was partially substituted by Pb. Also here the crystal was in the underdoped regime. To our knowledge, for samples in the overdoped regime no THz emission has been observed so far. One thus wonders whether or not there is an optimal charge carrier concentration for THz emission, and how both the electromagnetic and thermal properties of the IJJ stacks change with doping. Unfortunately, even for a given charge carrier concentration there is a large sample-to-sample variation of the THz emission properties, making systematic investigations difficult.

For small stacks, with lateral dimensions of a few μm consisting of some 10 IJJs, it was shown that the charge carrier concentration can be changed reversibly *in situ* by heavy current injection [62–65]. The effect is different from electromigration and oxygen diffusion and presumably related to the (un)filling of charge traps in the insulating layers [62, 63]. Using current injection both doping (increase of charge carrier concentration) and undoping (decrease of charge carrier concentration) is possible. To change the doping state of a sample the voltage V across the stack needs to exceed some threshold value V_t, which—for small stacks—is of the order of 1.3 V for doping and 1.7 V for undoping [62]. V_t is only weakly dependent on the number of junctions in the stack. Above V_t, for a fixed current the carrier concentration changes gradually, which is reflected in a change in V as a function of time. The c-axis resisitivity of BSCCO increases with decreasing charge carrier concentration. Thus, doping is observed as a decrease in V while undoping appears as an increase of V. The exact bias conditions for doping/undoping can in fact be complicated [63] and may depend on the stack type. For voltages below threshold the change in carrier concentration is persistent at low temperatures. Even at room temperature it changes only slowly, on the time scale of days.

The motivation of the present work was to study if charge carrier injection can also be employed for the large stacks used for THz generation and to what extent THz emission properties are affected by carrier injection. For these stacks currents of order 100 mA or larger need to be applied to reach V_t, leading to a Joule heat load of 150 mW or even more. This is two orders of magnitude larger than the heat load produced for 'small' mesas. In [62] it was mentioned that for large mesas containing 1000 IJJs undoping started at voltages of about 2.5 V but no details were given. As we will show both doping and undoping is possible for the large stacks under study, although the margins against destroying the sample are tight. We will also see that even moderate (un)doping strongly affects the THz emission properties. On purpose, the overall change in carrier concentration has been kept low, in order to systematically follow its impact on THz emission. Surprisingly, the highest emission power was found after *doping*, i.e. for the largest charge carrier concentration studied.

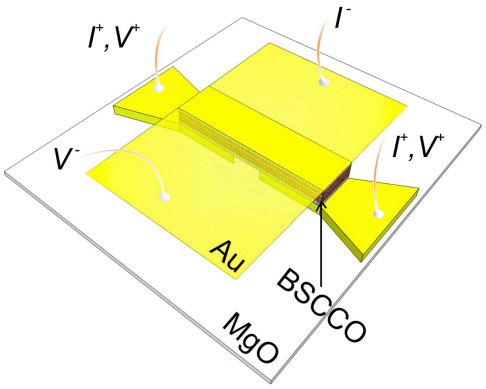

Figure 1. Sketch of the three-terminal stand-alone intrinsic Josephson junction stack used for the charge carrier injection experiments.

2. Samples and measurements

Doping and undoping experiments were performed on two mesas (lateral size: $70 \times 330\,\mu m^2$, critical temperature $T_c \approx 87$ K, junction number $N \approx 700$), and on two GBG structures contacted in a three-terminal configuration (lateral size: $50 \times 300\,\mu m^2$, $T_c \approx 88$ K, junction number $N \approx 930$). Undoping worked for all stacks, while doping was achieved for one mesa and one GBG structure. The overall (un)doping induced changes in T_c were below 1 K. For the mesas the overall THz emission power was very weak, although doping dependent. The THz emission power of the GBG structures was stronger. In the following we thus discuss data from these GBG structures, denoted stack 1 and 2.

The GBG structures are patterned in one step from the same single crystal which is near optimal doping. The stack geometry is sketched in figure 1. The sample preparation is similar to the one described in [26]. First, the crystal is glued with epoxy onto a Si substrate. Using a mechanical exfoliation method a fresh surface is created and a 120 nm Au layer as electrode is evaporated on this surface immediately after exfoliation. For each stack a $50 \times 330\,\mu m^2$ rectangular pattern with two injecting ports is transfered to the photoresist on the surface of the crystal by photolithography. After a mesa is formed by ion milling, the Au layer is removed partially in the middle of the rectangle with a KI solution to separate the two injectors. Then an MgO substrate is glued to the top of the

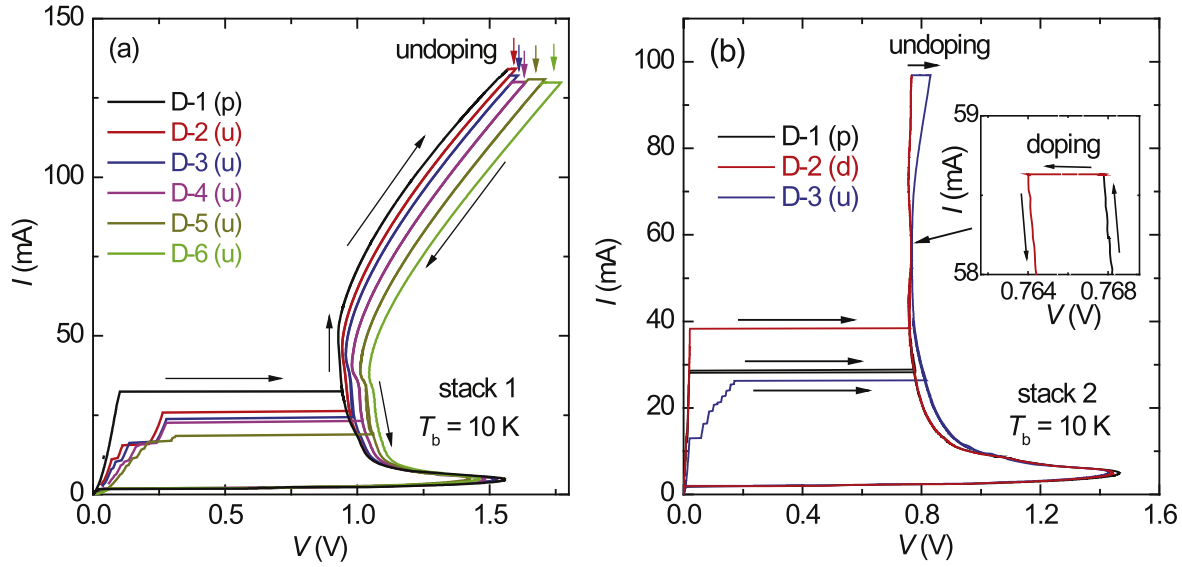

Figure 2. IVCs of (a) stack 1 and (b) stack 2 demonstrating the procedure of charge carrier injection. Curves labeled D-1, D-2 etc correspond to different doping states, starting with the pristine sample. Labels (p), (u) and (d) repectively indicate the pristine sample, undoping and doping. Bias conditions where (un)doping occurs are indicated. Measurements were performed at $T_b = 10$ K.

mesa with epoxy. The two substrates are separated, making the stacks stand alone on the MgO substrate. After a second exfoliation step another 30 nm thick Au layer is deposited on this stack as a ground terminal. A second photolithography and ion milling step is performed to remove the residual BSCCO on the injectors. The gap on the bottom Au layer between two injectors is about 75 μm wide. The thickness of both stacks is 1.4 μm, corresponding to $N \approx 930$ IJJs.

For the transport and emission measurements the samples were mounted inside an optical cryostat. The THz radiation was collected by parabolic mirrors and detected by a Ge bolometer. The *c*-axis resistance R was recorded as a function of bath temperature T_b, followed by a simultaneous measurement of the IVC and the emitted power at $T_b = 10$ K. Subsequently the current through the stack was strongly increased until either doping or undoping set in. After some hold time the current was reduced to zero. Measurements of R versus T_b and subsequently IVC and THz emission measurements were performed for the new doping level. This cycle was repeated several times until finally the sample got destroyed. For undoping a typical hold time was 0.5–1 h, precise numbers depending on the bias current and voltage V. For doping an initial decrease of V was seen at hold times of around 5 min, with a subsequent saturation of V for larger hold times.

For the measurements on stack 1 the two electrodes contacting the bottom of the stack were biased symmetrically; for the measurements on stack 2 only one of the split electrodes was used for current injection. The other was used as a voltage contact.

3. Results

To explain the procedure of charge carrier injection, figure 2(a) shows IVCs for stack 1. The stack was measured in a symmetrically biased two-terminal configuration, thus the contact resistances of the bottom and top electrodes to the BSCCO stack appear in the IVCs. Different colors distinguish IVCs for different doping states. The curve labeled D-1 is for the pristine sample. When increasing the current from zero one obtains near $I = 35$ mA an (instantaneous) switch from the zero voltage state of all IJJs to the fully resistive state, where all IJJs are in their resistive state. From the value of the switching current one infers a critical supercurrent density j_c of about 230 A cm^{-2}, which is in fact a factor of 4–5 lower than the critical supercurrent densities found for small-sized stacks [65]. For the large stacks used for THz generation it is likely that self-field effects limit j_c. When sweeping the current back and forth the fully resistive branch is reproducible, as long as the current is kept well below 130 mA. Undoping was performed at $I \approx 135$ mA, where $V \approx 1.56$ V. Here, V slowly drifts to larger voltages. When I is decreased after some hold time (45 min in this case) one obtains a new resistive branch (denoted D-2) representing a new doping state, with a decreased charge carrier density. In figure 2(a) the undoping process is perfomed 5 times, yielding IVCs labeled D-2 to D-6. Note that there are multiple switching steps on IVCs D-2 to D-6, indicating that upon undoping the stack becomes increasingly inhomogeneous.

Figure 2(b) shows IVCs for stack 2 for two charge carrier injection runs. Only one of the split electrodes was used for current bias, while the other was used for measuring V, i.e. a three terminal configuration was employed eliminating the contact resistance between the bottom current injection electrode and the stack. Curve D-1 shows the IVC for the pristine sample. The switch from the superconducting state to the fully resistive state occurs at $I = 28$ mA. Doping was achieved at $I \approx 59$ mA and $V \approx 0.77$ V. The corresponding IVC is labeled D-2. In fact, the change in V during the 30 min hold time was very modest at this bias, probably preventing to find the bias condition for doping for some of the other stacks.

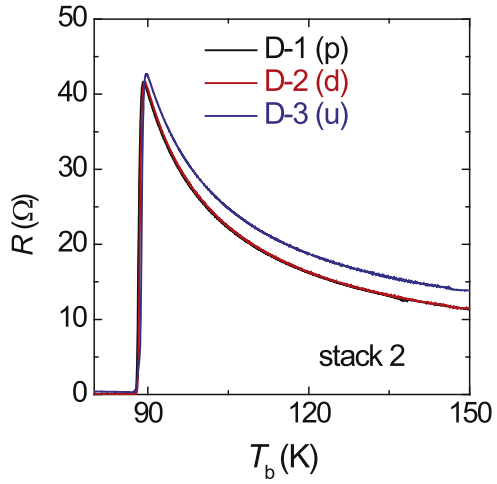

Figure 3. Temperature dependence of *c*-axis resistance for stack 2 for the pristine sample (D-1), after a doping step (D-2) and after subsequent undoping (D-3).

Further, note that the switching current from the superconducting state to the resistive state is now at 38 mA, i.e. by a factor of 1.4 higher than for IVC D-1. Like for the pristine state only a single switching step was observed, indicating that the doping procedure did not increase the sample inhomogeneity. Finally, at $I = 97$ mA undoping started and during undoping, with a hold time of 40 min, the voltage increased from 0.77 V to 0.83 V. The IVC for this new doping level is labeled D-3. On this curve, like for states D-2 to D-6 of stack 1, one observes multiple switching steps.

For bias currents below 40 mA the resistive branches of the three IVCs do not differ strongly from each other, indicating that the (low temperature) interlayer resistance has not changed very much during doping and undoping. This is also reflected in figure 3 showing R versus T_b curves for the three doping levels of stack 2. Curves for doping states D-1 and D-2 basically coincide, while for D-3 R is slightly higher, the difference to the D-1 and D-2 curves growing with increasing temperature. The critical temperatures for curves D-1 to D-3 differ by less than 0.5 K, which is within the error bars of the thermometer and consistent with the fact that the pristine sample was near optimal doping. Further, by comparing R versus T_b with V/I taken from the IVCs during undoping, we estimate that the stack temperature during undoping was around 200–250 K. Also for stack 1 the change in T_c was below 1 K. Thus, for both stacks and all (un)doping procedures the hole concentration was in the range 0.16 ± 0.01 holes per Cu atom.

Also note that in figure 2 the back-bending of the IVCs starting near $I = 5$ mA occurs at voltages V_{max} which are comparable (stack 1) or significantly larger (stack 2) than the high-current threshold voltages V_t for doping and undoping. We never found (un)doping effects in the low-bias region near V_{max}, where the hot spot has not yet formed and, according to simulations [60, 61], the temperature in the stack exceeds T_b by less than 40 K. Thus, either V_t strongly decreases with increasing temperature or a large current is needed in addition to start the (un)doping processes.

Let us now turn to the THz emission properties. For both samples emission occurred at currents below 10 mA, and this regime is shown in figure 4 for stack 1 and in figure 5 for stack 2. Figure 4(a) displays IVCs for doping state D-1 (pristine sample) and undoped states D-2, D-3, D-5 and D-6. In the back-bending region of the IVCs, i.e., for currents between 6 and 10 mA, the emission power P_e is very low for the pristine stack, rises for doping states D-2 and D-3 and is again almost absent for doping states D-4 and D-5, see figure 4(b). In this regime, there are peaks in P_e versus I which occur at very different currents for the different doping states. For currents between 4 and 6 mA, i.e. near V_{max}, only the pristine stack showed noticeable radiation, see figure 4(b). For currents between 2 and 4 mA the highest emission power was much stronger than for larger bias currents. In the low-bias regime, the emission data for the different doping states are best resolved in the P_e versus V plot, see figure 4(c). The highest values of P_e are observed for voltages below $V = 1$ V. Here, jumps in the IVCs indicate that some of the junctions have switched back to their superconducting state. Thus, the number of junctions in the resistive state varies, making it difficult to compare P_e for the different doping states. On the other hand, for voltages above 1.1 V for doping states D-1 to D-3, and above 0.98 V for doping states D-5 and D-6, no switch-back was detectable and presumably all IJJs were in their resistive state. For the pristine stack there is a peak in P_e near $V = 1.19$ V. For the marginally different doping states D-2 and D-3 one observes an emission peak near 1.15 V. At this voltage the IVC exhibits a bump indicating that an electromagnetic cavity mode has been excited. Such bumps in the IVCs of IJJ stacks have been observed before, see e.g. [2]. In figure 4 we have drawn a vertical line between graphs (a) and (c) to show that the bumps on the IVCs and the emission peaks for doping states D-2 and D-3 occur at the same voltage. A peak in P_e versus V and a corresponding bump in the IVC is also observed for doping state D-6, see left vertical line between figures 4(a) and (c). The emission peak in fact is asymmetric and may consist of a double-peak structure with peak voltages near 1.12 V and 1.06 V, respectively. For doping state D-5 an emission peak and a corresponding bump in the IVC occurs near $V = 1.02$ V. A possible explanation for the peaks and bumps and their variation for different doping states is that in the series D-1 to D-6 two different resonances have been excited. The voltage position of the peak seems to shift to lower values for the series D-1 to D-5. In a first approach one may associate the observed shift with a change in contact resistance during the various undoping steps. Indeed, as can be seen from figure 4(a) the contact resistance increases during undoping, from about 4.6 Ω for the pristine stack to about 15 Ω for doping state D-6. However, if one corrected the IVCs for the contact resistances the voltage shift in the bumps and peaks would *increase* rather than decrease. The shift thus needs further discussion.

For stacks 1 and 2 we do not have frequency resolved emission spectra but for other samples we found that in the fully resistive state and in particular also near bumps in the IVC almost all IJJs participate in radiation. We have also seen before that the bumps in the IVCs shift towards lower

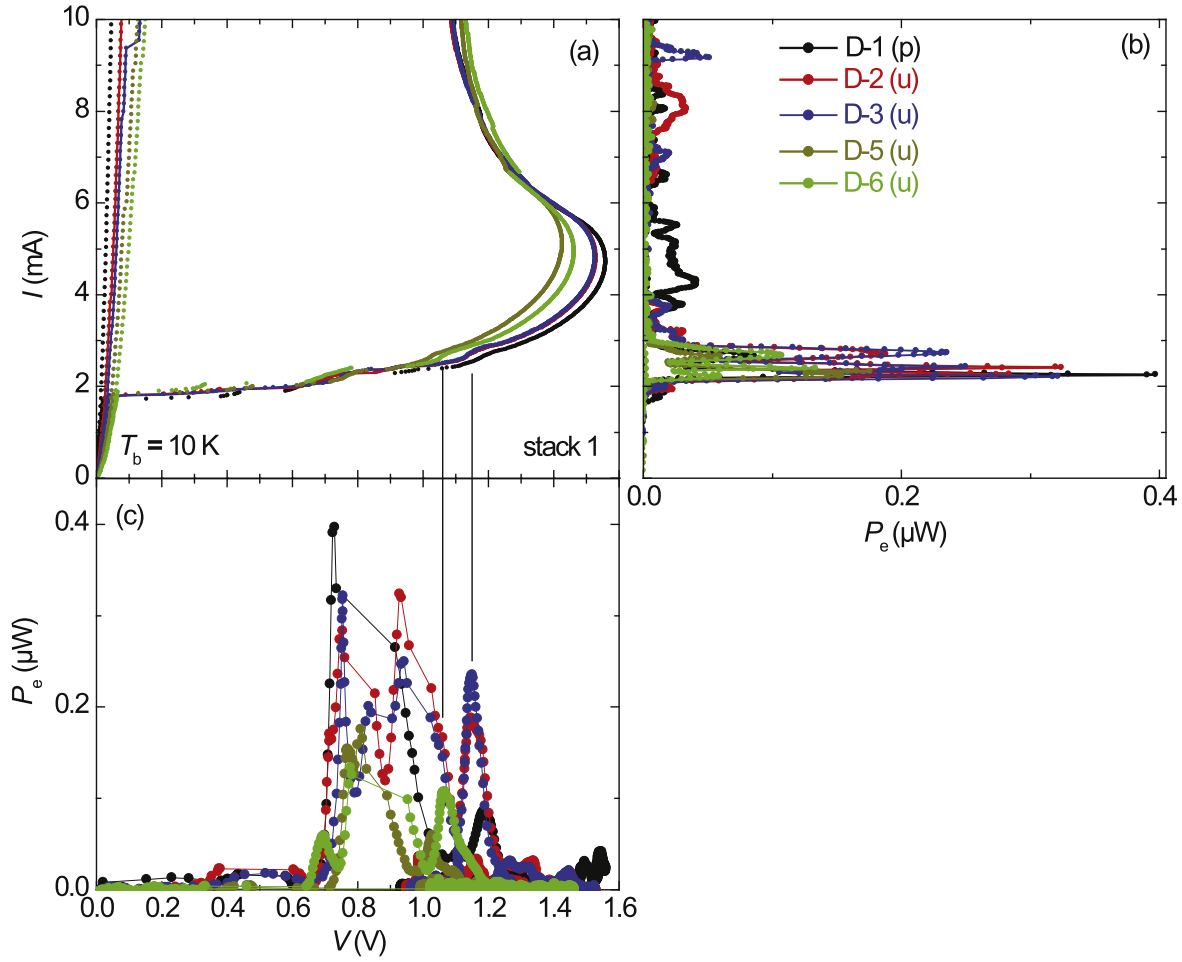

Figure 4. THz emission properties of stack 1, measured at $T_b = 10$ K for the 5 doping states indicated: (a) IVCs, (b) emitted power P_e versus I and (c) emitted power P_e versus V. Vertical lines between (a) and (c) are a guide to the eye indicating peaks in P_e versus V and corresponding bumps in the IVCs. Labels (p) and (u) indicate the pristine sample (p) and different runs of undoping (u).

voltages when increasing the bath temperature. A similar effect may work for stack 1. In the series D-1 to D-6 the hole carrier concentration decreases and the c-axis resistivity at given temperature increases. The c-axis resistivity at given hole carrier concentration strongly increases with decreasing temperature for underdoped samples and also near optimal doping. For a given current I and bath temperature this implies that the increase in resistance with decreasing charge carrier concentration can be over-compensated by the decrease of R due to the local temperature increase arising from Joule heating. The (in-phase) cavity resonance frequency is proportional to the mode velocity c_1 which decreases with increasing temperature, see e.g. [60]. We thus expect a decrease in the cavity mode resonance frequencies with increasing stack temperature. To explain the shift in the bumps in the IVCs and of the peaks in P_e versus V one may also consider a doping dependence of the dielectric constant ε and consequently of the diffraction index. Such a dependence was derived from measurements of the Josephson plasma frequency [66]. Near optimal doping ε decreases weakly with decreasing hole concentration. One would thus expect an *increase* of the cavity resonance frequency for the series D-1 to D-6.

Apart from such details the basic message of the overall figure 4 is that THz emission properties enormously depend on the doping state of the sample even for the modest changes we have introduced within our undoping sequence. This conclusion can also be given for the case of stack 2, for which THz emission data are shown in figure 5. For this stack THz emission occurred for currents below 8.5 mA. The highest emission power was detected for doping state D-2, which is remarkable since, typically, IJJ stacks fabricated from slightly underdoped crystals emit best. A possible reason could be an improvement of the local sample homogeneity during doping. As can be seen from a comparison of figures 5(a) and (c), both for the pristine stack and for doping state D-2 the highest emission occurred at voltages where some of the junctions have returned to their superconducting state. For currents between 5 and 8.5 mA, i.e. in the back-bending region of the IVCs peaks exhibiting some fine structures can be observed in P_e versus I. For all doping states there is a broad emission peak between 5.3 and 7 mA which has about the same amplitude for doping states D-1 and D-2 and a much smaller one for doping state D-3. Another peak is visible for all three doping states for currents in the low-bias regime near 3 mA and voltages near 1.05 V, see figure 5(c). Like for stack 1

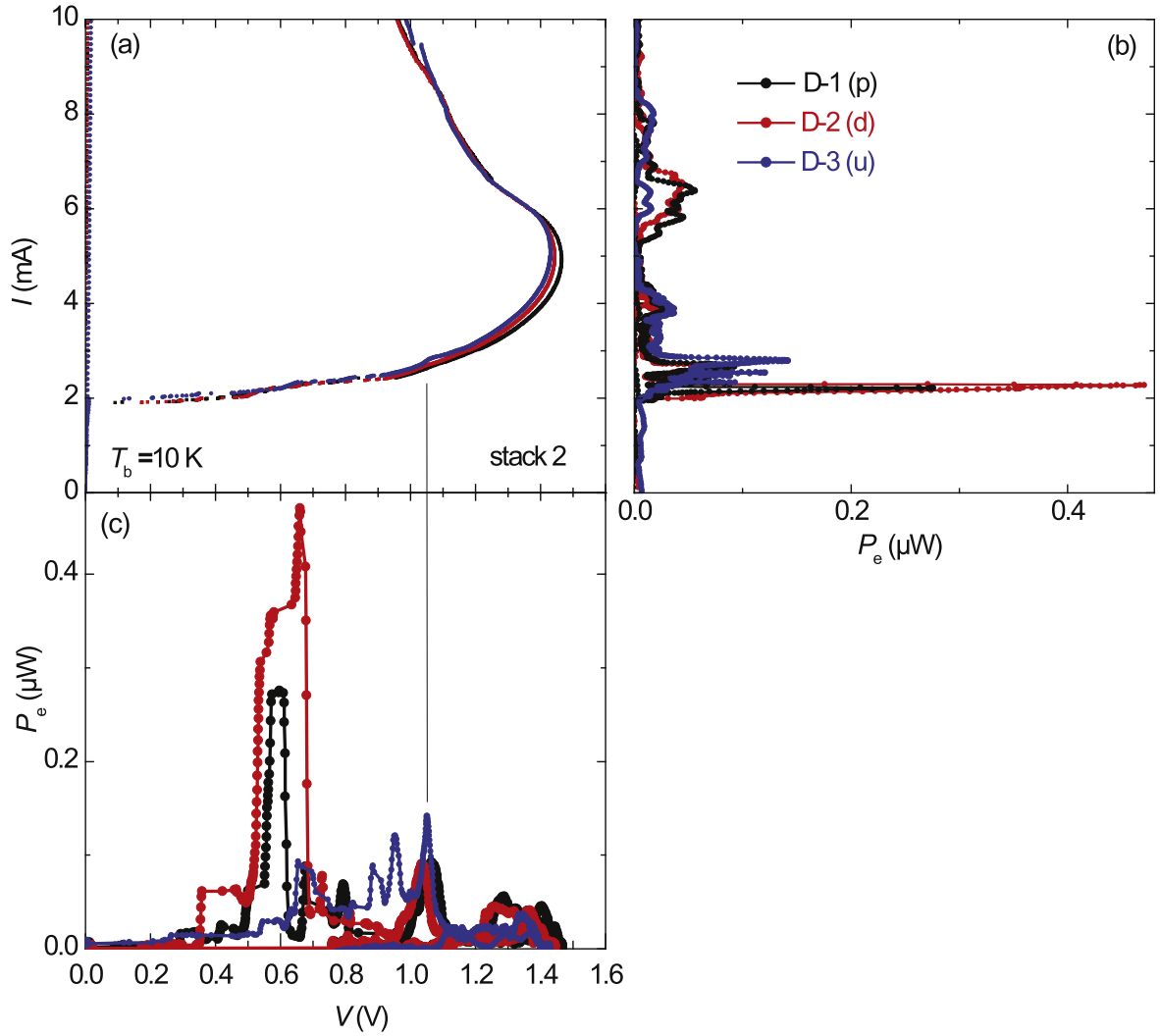

Figure 5. THz emission properties of stack 2, measured at $T_b = 10$ K for doping states D-1 to D-3. (a) IVCs, (b) emitted power P_e versus I and (c) emitted power P_e versus V. Vertical line between (a) and (c) is a guide to the eye indicating peaks in P_e versus V and corresponding bumps in the IVCs. Labels (p), (d) and (u) indicate the pristine (p), doped (d) and undoped (u) sample.

there is also an associated bump in the IVC, as indicated by the vertical line between figures 5(a) and (c). Both the peaks and the bumps are located at sligthly different voltage positions for the three doping states, the shift explainable as an effect of the change in local temperature. For doping state D-3 there are also emission peaks at 0.89 V and at 0.95 V. These peaks, observed in the fully resistive state of the sample, are absent for doping states D-1 and D-2.

4. Conclusions

In summary we have shown that doping by carrier injection is feasible also for the large IJJ stacks used for THz generation. Both doping and undoping has been demonstrated. Even moderate changes in the charge carrier concentration introduce large changes in the THz emission properties. This is our main message, giving a proof-of-principle that doping by carrier injection can be used to systematically modify and study the THz emission properties of such stacks. For example, we found the emission to be largest after *doping* the pristine sample. This was unexpected since, typically, best emission properties are found for slightly underdoped IJJ stacks. The observed improvement in emission power may be related to an improvement of sample inhomogeneities during the doping step.

In the present work we have intentionally altered the doping states of our samples only in a small range near optimal doping. However, extending doping and undoping studies of large THz emitting stacks over a wide range of charge carrier concentrations is possible in principle and may show the limits and optima of the THz emission properties of IJJ stacks with respect to charge carrier concentration.

Acknowledgments

We gratefully acknowledge financial support by the National Natural Science Foundation of China (Grant Nos. 11234006,

61501220), the Priority Academic Program Development of Jiangsu Higher Education Institutions, Jiangsu Provincial Natural Science Fund (BK20150561), the Deutsche Forschungsgemeinschaft (Project KL930/13-2), JSPS KAKENHI Grant Number 25289108, RFBR grant 14-02-91335, EU-FP6-COST Action MP1201 and by the Scientific and Technological Research Council of Turkey under contract no. TUBITAK (2219)-1059B191501336.

References

[1] Kleiner R, Steinmeyer F, Kunkel G and Müller P 1992 *Phys. Rev. Lett.* **68** 2394
[2] Ozyuzer L *et al* 2007 *Science* **318** 1291
[3] Welp U, Kadowaki K and Kleiner R 2013 *Nat. Photon.* **7** 702
[4] Kakeya I and Wang H 2016 *Supercond. Sci. Technol.* **29** 073001
[5] Wang H B, Guénon S, Yuan J, Iishi A, Arisawa S, Hatano T, Yamashita T, Koelle D and Kleiner R 2009 *Phys. Rev. Lett.* **102** 017006
[6] Guénon S *et al* 2010 *Phys. Rev.* B **82** 214506
[7] Kurter C, Ozyuzer L, Proslier T, Zasadzinski J F, Hinks D G and Gray K E 2010 *Phys. Rev.* B **81** 224518
[8] Wang H B *et al* 2010 *Phys. Rev. Lett.* **105** 057002
[9] Tsujimoto M, Yamaki K, Deguchi K, Yamamoto T, Kashiwagi T, Minami H, Tachiki M, Kadowaki K and Klemm R A 2010 *Phys. Rev. Lett.* **105** 037005
[10] Benseman T M, Koshelev A E, Gray K E, Kwok W-K, Welp U, Kadowaki K, Tachiki M and Yamamoto T 2011 *Phys. Rev.* B **84** 064523
[11] Yuan J *et al* 2012 *Supercond. Sci. Technol.* **25** 075015
[12] Li M Y *et al* 2012 *Phys. Rev.* B **86** 060505(R)
[13] Kakeya I, Omukai Y, Yamamoto T, Kadowaki K and Suzuki M 2012 *Appl. Phys. Lett.* **100** 242603
[14] Tsujimoto M, Minami H, Delfanazari K, Sawamura M, Nakayama R, Kitamura T, Yamamoto T, Kashiwagi T, Hattori T and Kadowaki K 2012 *J. Appl. Phys.* **111** 123111
[15] Tsujimoto M *et al* 2012 *Phys. Rev. Lett.* **108** 107006
[16] Kashiwagi T *et al* 2012 *Japan. J. Appl. Phys.* **51** 010113
[17] An D Y *et al* 2013 *Appl. Phys. Lett.* **102** 092601
[18] Benseman T M, Koshelev A E, Kwok W-K, Welp U, Vlasko-Vlasov V K, Kadowaki K, Minami H and Watanabe C 2013 *J. Appl. Phys.* **113** 133902
[19] Benseman T M, Gray K E, Koshelev A E, Kwok W-K, Welp U, Minami H, Kadowaki K and Yamamoto T 2013 *Appl. Phys. Lett.* **103** 022602
[20] Sekimoto S, Watanabe C, Minami H, Yamamoto T, Kashiwagi T, Klemm R A and Kadowaki K 2013 *Appl. Phys. Lett.* **103** 182601
[21] Minami H, Watanabe C, Sato K, Sekimoto S, Yamamoto T, Kashiwagi T, Klemm R A and Kadowaki K 2014 *Phys. Rev.* B **89** 054503
[22] Ji M *et al* 2014 *Appl. Phys. Lett.* **105** 122602
[23] Tsujimoto M, Kambara H, Maeda Y, Yoshioka Y, Nakagawa Y and Kakeya I 2014 *Phys. Rev. Appl.* **2** 044016
[24] Watanabe C *et al* 2015 *Appl. Phys. Lett.* **106** 042603
[25] Zhou X J *et al* 2015 *Phys. Rev. Appl.* **3** 044012
[26] Zhou X J *et al* 2015 *Appl.Phys. Lett.* **107** 122602
[27] Hao L *et al* 2015 *Phys. Rev. Appl.* **3** 024006
[28] Gross B *et al* 2015 *Supercond. Sci. Technol.* **28** 055004
[29] Kakeya I, Hirayama N, Omukai Y and Suzuki M 2015 *J. Appl. Phys.* **117** 043914
[30] Kashiwagi T *et al* 2015 *Appl. Phys. Lett.* **107** 082601
[31] Kashiwagi T *et al* 2015 *Phys. Rev. Appl.* **4** 054018
[32] Benseman T M *et al* 2015 *Phys. Rev. Appl.* **3** 044017
[33] Tsujimoto M, Maeda Y, Kambara H, Elarabi A, Yoshioka Y, Nakagawa Y, Wen Y, Doi T, Saito H and Kakeya I 2015 *Supercond. Sci. Technol.* **28** 105015
[34] Watanabe C, Minami H, Kitamura T, Saiwai Y, Shibano Y, Katsuragawa T, Kubo H, Kashiwagi T, Klemm R A and Kadowaki K 2016 *Supercond. Sci. Technol.* **29** 065022
[35] Nakade K, Kashiwagi T, Saiwai Y, Minami H, Yamamoto T, Klemm R A and Kadowaki K 2016 *Sci. Rep.* **6** 23178
[36] Tsujimoto M, Maeda Y, Elarabi A, Yoshioka Y, Nakagawa Y, Wen Y, Doi T, Saito H and Kakeya I 2016 *Opt. Express* **24** 4591
[37] Bulaevskii L N and Koshelev A E 2007 *Phys. Rev. Lett.* **99** 057002
[38] Lin S and Hu X 2008 *Phys. Rev. Lett.* **100** 247006
[39] Krasnov V M 2009 *Phys. Rev. Lett.* **103** 227002
[40] Tachiki M, Fukuya S and Koyama T 2009 *Phys. Rev. Lett.* **102** 127002
[41] Pedersen N and Madsen S 2009 *IEEE Trans Appl. Supercond.* **19** 726
[42] Hu X and Lin S Z 2009 *Phys. Rev.* B **80** 064516
[43] Koyama T, Matsumoto H, Machida M and Kadowaki K 2009 *Phys. Rev.* B **79** 104522
[44] Klemm R A and Kadowaki K 2010 *J. Phys.: Condens. Matter* **22** 375701
[45] Klemm R A and Kadowaki K 2010 *J. Supercond. Nov. Magn.* **23** 613
[46] Krasnov V M 2010 *Phys. Rev.* B **82** 134524
[47] Koshelev A E 2010 *Phys. Rev.* B **82** 174512
[48] Katterwe S O, Rydh A, Motzkau H, Kulakov A B and Krasnov V M 2010 *Phys. Rev.* B **82** 024517
[49] Yurgens A A 2011 *Phys. Rev.* B **83** 184501
[50] Koyama T, Matsumoto H, Machida M and Ota Y 2011 *Supercond. Sci. Technol.* **24** 085007
[51] Krasnov V M 2011 *Phys. Rev.* B **83** 174517
[52] Yurgens A A and Bulaevskii L N 2011 *Supercond. Sci. Technol.* **24** 015003
[53] Gross B *et al* 2012 *Phys. Rev.* B **86** 094524
[54] Asai H, Tachiki M and Kadowaki K 2012 *Phys. Rev.* B **85** 064521
[55] Lin S and Hu X 2012 *Phys. Rev.* B **86** 054506
[56] Grib A and Seidel P 2012 *Low Temp. Phys.* **38** 321
[57] Gross B *et al* 2013 *Phys. Rev.* B **88** 014524
[58] Liu F, Lin S Z and Hu X 2013 *Supercond. Sci. Technol.* **26** 025003
[59] Asai H and Kawabata S 2014 *Appl. Phys. Lett.* **101** 112601
[60] Rudau F *et al* 2015 *Phys. Rev.* B **91** 104513
[61] Rudau F *et al* 2016 *Phys. Rev. Appl.* **5** 044017
[62] Koval Y, Jin X, Bergmann C, Simsek Y, Ozyuzer L, Müller P, Wang H B, Behr G and Büchner B 2010 *Appl. Phys. Lett.* **96** 082507
[63] Motzkau H, Jacobs T, Katterwe S-O, Rydh A and Krasnov V M 2012 *Phys. Rev.* B **85** 144519
[64] Kizilaslan O, Simsek Y, Aksan M A, Koval Y and Müller P 2015 *Supercond. Sci. Technol.* **28** 085017
[65] Jacobs T, Simsek Y, Koval Y, Müller P and Krasnov V M 2016 *Phys. Rev. Lett.* **116** 067001
[66] Müller P 2016 in preparation